The life of an mRNA in space and time

Ya'ara Ben-Ari[1,*], Yehuda Brody[1,*], Noa Kinor[1], Amir Mor[1], Toshiro Tsukamoto[2], David L. Spector[3], Robert H. Singer[4] and Yaron Shav-Tal[1,‡]

[1]The Mina and Everard Goodman Faculty of Life Sciences and Institute of Nanotechnology, Bar-Ilan University, Ramat Gan 52900, Israel
[2]Department of Dermatology, Chiba University Graduate School of Medicine, Chuo-ku, Chiba 260-8670, Japan
[3]Cold Spring Harbor Laboratory, One Bungtown Road, Cold Spring Harbor, NY 11724, USA
[4]Department of Anatomy and Structural Biology, Albert Einstein College of Medicine, Bronx, NY 10461, USA

*These authors contributed equally to this work
‡Author for correspondence (shavtaly@mail.biu.ac.il)

Accepted 6 March 2010
Journal of Cell Science 123, 1761-1774

doi:10.1242/jcs.062638

Summary

Nuclear transcribed genes produce mRNA transcripts destined to travel from the site of transcription to the cytoplasm for protein translation. Certain transcripts can be further localized to specific cytoplasmic regions. We examined the life cycle of a transcribed β-actin mRNA throughout gene expression and localization, in a cell system that allows the in vivo detection of the gene locus, the transcribed mRNAs and the cytoplasmic β-actin protein that integrates into the actin cytoskeleton. Quantification showed that RNA polymerase II elongation progressed at a rate of 3.3 kb/minute and that transactivator binding to the promoter was transient (40 seconds), and demonstrated the unique spatial structure of the coding and non-coding regions of the integrated gene within the transcription site. The rates of gene induction were measured during interphase and after mitosis, demonstrating that daughter cells were not synchronized in respect to transcription initiation of the studied gene. Comparison of the spatial and temporal kinetics of nucleoplasmic and cytoplasmic mRNA transport showed that the β-actin-localization response initiates from the existing cytoplasmic mRNA pool and not from the newly synthesized transcripts arising after gene induction. It was also demonstrated that mechanisms of random movement were predominant in mediating the efficient translocation of mRNA in the eukaryotic cell.

Key words: mRNA dynamics, Gene expression, Transcription, Live cell imaging

Introduction

The control of gene expression in eukaryotes is a complex and highly regulated process involving numerous steps. During transcription, pre-mRNAs are cotranscriptionally processed by the capping, splicing and polyadenylation machineries (Bentley, 2005; Hirose and Manley, 2000; Maniatis and Reed, 2002; Moore and Proudfoot, 2009; Neugebauer, 2002). The mature mRNA is primed for export, travels to the nuclear envelope and translocates into the cytoplasm (Kohler and Hurt, 2007). Certain mRNA species can undergo an additional process of mRNA localization that enables the migration of translationally silenced mRNAs to specific cellular destinations for subsequent translation (Shav-Tal and Singer, 2005). The β-actin gene (*ACTB*) is a housekeeping gene; in mammalian cells, its mRNA undergoes localization to the leading edge of migrating cells (Condeelis and Singer, 2005). Chicken β-actin mRNA localization was detected in 30-35% of chick embryonic cells (Latham et al., 1994; Lawrence and Singer, 1986). A correlation between the localization of the β-actin mRNA and the localized production of the β-actin protein is found in actin-rich protruding cellular structures, such as microvilli and the leading edge of moving cells (Hofer et al., 1997; Shestakova et al., 2001). The β-actin mRNA contains 'zipcode' sequences in the 3′-untranslated region (3′-UTR) that are responsible for mRNA targeting (Kislauskis et al., 1993). These sequences are immediately downstream of the stop codon and recruit the zipcode-binding protein ZBP1 through interactions with its K homology (KH) domains (Ross et al., 1997). β-actin mRNA can travel on actin filaments (Sundell and Singer, 1991) and localizes to the leading edge of migrating fibroblasts (Lawrence and Singer, 1986). In neurons, it travels on microtubules (Bassell et al., 1994). ZBP1 represses the translation of β-actin mRNA until it reaches actin-rich areas, such as filopodia and growth cones. This repression is reversed by phosphorylation (Huttelmaier et al., 2005).

Understanding the kinetics of mRNA translocation, from the point of transcription, through nuclear transport, localization, translation and degradation, is of fundamental interest because gene expression is regulated at all different levels of this pathway (Moore, 2005). Kinetic information on real-time gene expression has increased with the development of live-cell imaging techniques and methods for labeling DNA and RNA in living cells (Shav-Tal et al., 2006). A number of studies have used the MS2 mRNA-tagging system to examine mRNA dynamics at specific points in the gene expression pathway. For instance, transcription kinetics were examined in mammalian cells (Darzacq et al., 2007; Janicki et al., 2004), *Escherichia coli* (Golding and Cox, 2004; Golding et al., 2005) and *Dictyostelium* (Chubb et al., 2006). The dynamics of translocation of mRNA-protein complexes (mRNPs) in either the nucleoplasm (Shav-Tal et al., 2004) or the cytoplasm (Fusco et al., 2003) were also studied.

To date, no study has followed and quantified the complete cellular pathway of a protein-coding mammalian mRNA in an in vivo cell system at both the spatial and temporal levels. To examine the kinetics of a functional mRNA from the time it is transcribed until it reaches its correct cytoplasmic location and is translated into a functional protein, we designed a cell system that is capable of live-cell visualization and amenable to examination of a functional gene, its mRNA product and the translated protein product, at the single-cell level. To this end, we used β-actin mRNA in light of its localization properties and

Journal of Cell Science

coding of a much-required protein product. Herein, we provide a combined spatial and temporal kinetic analysis of β-actin mRNA dynamics in vivo in both nuclear and cytoplasmic compartments.

Results

Generation of a gene construct for following β-actin mRNA in vivo

To enable the visualization of the β-actin gene, the transcribed mRNA and the translated protein in live-cell experiments, a gene construct was prepared that included the β-actin-coding sequence together with elements that enable the real-time tagging and detection of a DNA sequence, mRNA and protein within the same cell (Fig. 1A). The gene was under inducible transcriptional control because we wished to follow the temporal distribution of the mRNAs from the initial point of transcription to them reaching the cytoplasm. Following is a description of the gene starting at the 5′ end. The tagging of the gene (DNA) was achieved by introducing a series of 256 *lac* operator (*lacO*) repeats to precede the β-actin-coding region (Tumbar et al., 1999). Coexpression with a fluorescently tagged *lac* repressor protein (RFP-LacI) that specifically binds to the *lacO* repeats allowed the detection of the genomic site of integration. Downstream was a series of 96 tetracycline responsive elements (TREs), which enabled inducible transcriptional control by the Tet-On system. In the presence of the reverse tetracycline transcriptional activator (rtTA or Tet-On) and doxycycline (dox), transcription was induced. The transcribed mRNA contained a coding region for CFP-tagged β-actin protein, so we could identify the translated protein, and also included the endogenous 3′-UTR of this mRNA, which contains the zipcode elements required for β-actin mRNA localization. A series of 24 MS2 repeat sequences was inserted into the gene between the β-actin-

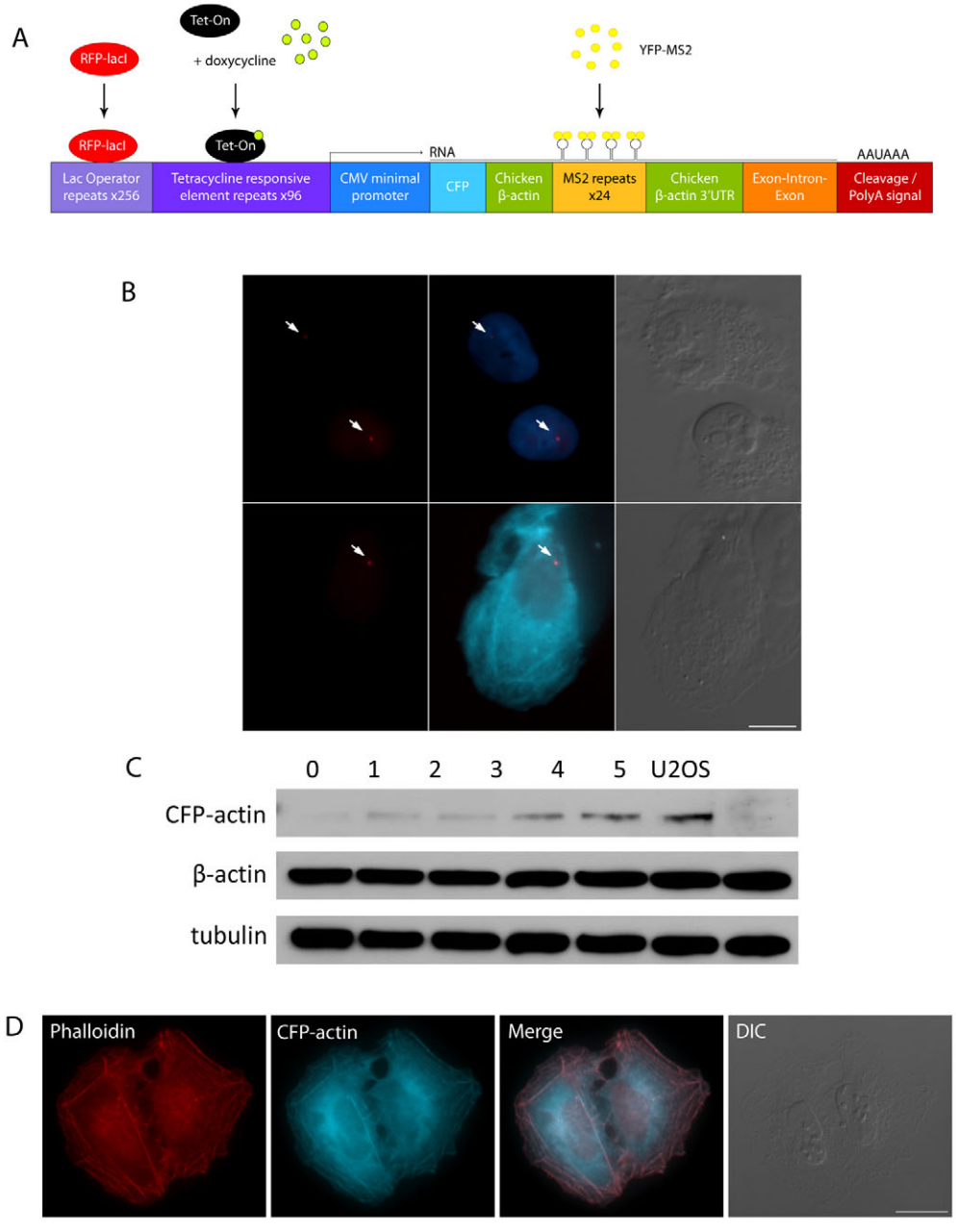

Fig. 1. Cell system for following β-actin gene expression in vivo. (**A**) Schematic of the gene construct. The 5′ end contains a series of 256 *lacO* repeats that bind RFP-LacI and mark the site of integration and transcription. Transcriptional induction from the minimal CMV promoter is achieved by the binding of reverse tetracycline transcriptional activator (rtTA or Tet-On) to TREs in the presence of dox. The transcribed mRNA contains the coding sequence for CFP–chicken-β-actin, 24 MS2 repeats that are bound by the YFP-MS2 fusion protein and the 3′-UTR of chicken β-actin, which contains the zipcode. At the 3′ end, a portion of a rabbit β-globin exon-intron-exon module is followed by a cleavage-polyA signal. (**B**) The selected cell clone contains a small gene integration site marked by RFP-LacI (red dots, white arrows). The nucleus in uninduced cells is in blue (top). In induced cells following dox-induced transcriptional activation, CFP-actin bundles are detected (bottom). Scale bar: 10 μm. (**C**) Western blot of CFP-actin in cells induced with dox for 1-5 hours showed protein accumulation, compared with no change in the levels of human β-actin or tubulin. (**D**) TRITC-phalloidin staining shows the integration of CFP-actin into filamentous actin. Scale bar: 20 μm.

coding region and the 3′-UTR. These MS2 repeats form stem-loop structures in the transcribed mRNA; each stem-loop is specifically bound by a dimer of a coexpressed YFP-MS2 protein. This results in prominent tagging of single mRNA molecules (mRNPs) as they are transcribed (Shav-Tal et al., 2004). Finally, the mRNA contained an intron to enable pre-mRNA processing. Altogether, in this fashion, we could visually identify the gene locus (*lacO* and LacI), the transcribed mRNA (YFP-MS2) and the translated protein (CFP-actin) in single living cells.

Generation of a transcriptionally inducible cell line for following β-actin mRNA in vivo

The gene construct was stably integrated into the U2OS Tet-On human cell line. Because we wanted to distinguish between the

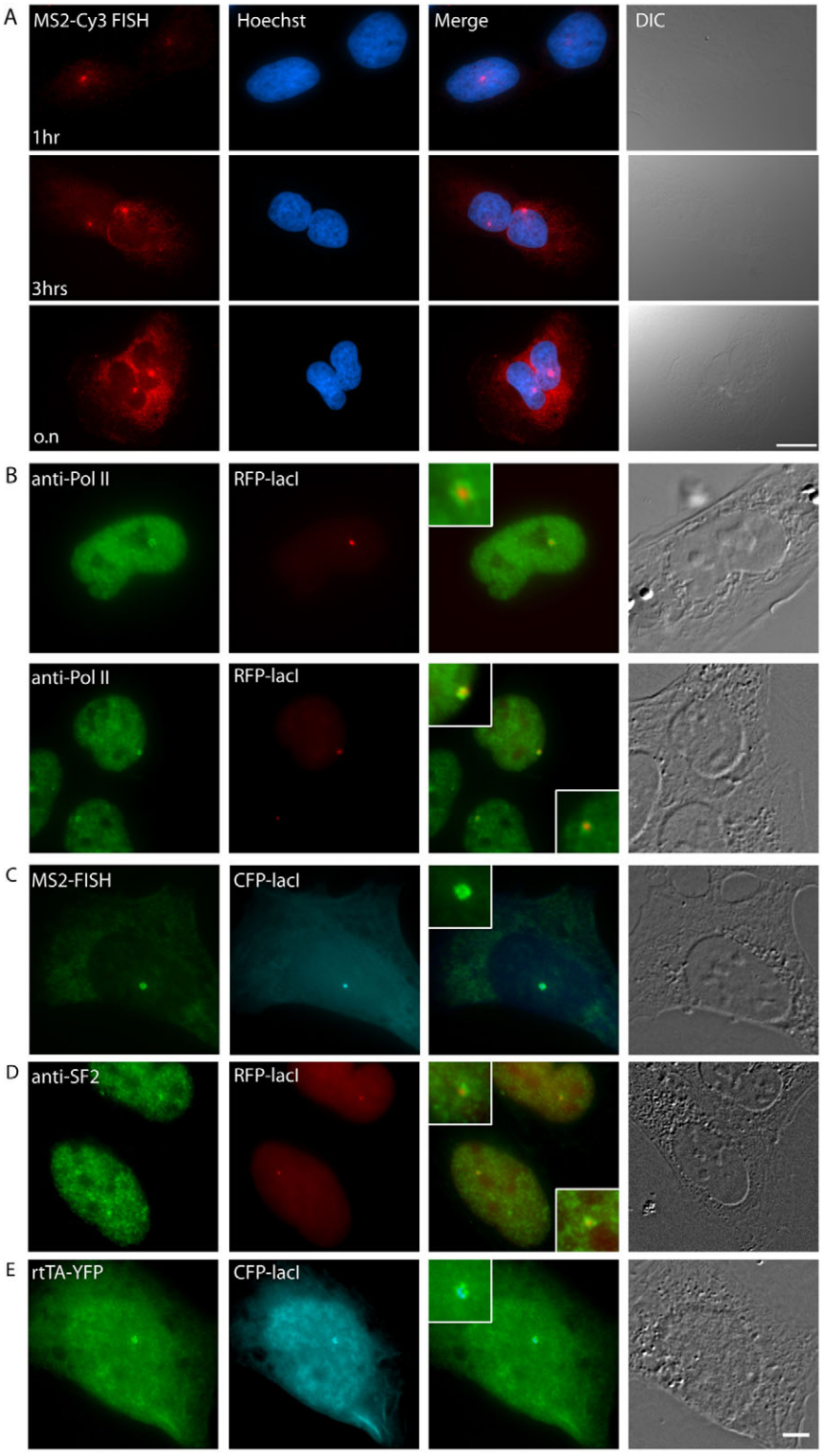

Fig. 2. Actively transcribing sequences surround the *lacO* sequences at the gene locus. (**A**) RNA-FISH with an MS2-Cy3 probe (red) shows the accumulation of β-actin–MS2 mRNA following transcriptional induction. Top and middle rows: 1 and 3 hour inductions show a transcription site and some cellular mRNAs. Bottom row: longer induction times show accumulation of cytoplasmic mRNAs (o.n. = overnight). Scale bars: 10 μm. (**B**) The transcriptionally active sequences encircle the non-coding *lacO* repeats, as seen by the recruitment of endogenous RNA Pol II (green) to the transcription site (RFP-LacI, red). (**C**) The nascent transcripts (MS2-Cy3 FISH, green), (**D**) the endogenous SF2/ASF splicing factor (green) and (**E**) the rtTA transactivator (green) all surround the gene locus (CFP- or RFP-LacI). Enlarged transcription sites are shown: red and green merges show active transcription (green) surrounding the locus (red). Green alone shows the circular structure of the active sequences. Scale bars: 5 μm.

endogenous human β-actin mRNA and the mRNA produced by our gene, we used the chicken mRNA region encoding β-actin and its 3′-UTR sequence. The chicken and human β-actin proteins are 100% identical, whereas their 3′-UTR sequences are ~50% similar, with 65% identity in the zipcode area (Kislauskis et al., 1994). After stable integration, single colonies were picked and cells were screened for CFP-actin expression, following dox-induced transcription. Positive cells that showed CFP-labeled cytoplasmic actin bundles were further screened for a small genomic gene-integration site, as detected by transient RFP-LacI expression.

Clone 43 was chosen for further study because it contained a small gene locus, indicating the integration of a relatively small gene-copy number. The number of integrated gene copies in the tandem gene array was six, as quantified by real-time PCR. Fig. 1B shows the detection of the genomic integration site in uninduced and in dox-induced cells (indicated by RFP-LacI), and the appearance of CFP-actin fibers in the induced cells. Whereas previous studies have demonstrated decondensation of the gene array upon transcriptional activation (Janicki and Spector, 2003; Tsukamoto et al., 2000; Tumbar et al., 1999), this was not resolvable in these cells, probably because of the low copy number in the gene array. Cytoplasmic CFP-actin was observed 2-3 hours following induction and was then seen to form actin bundles detectable at 5-6 hours post-induction. The expression of CFP-actin in the cells in comparison to the endogenous β-actin protein was examined by western blotting; an increase in CFP-actin levels could be observed over the course of 5 hours that did not interfere with endogenous β-actin levels (Fig. 1C). The CFP-actin protein exhibited a characteristic cytoskeletal pattern and co-integration into the endogenous actin cytoskeleton was verified using phalloidin staining (Fig. 1D). Prolonged expression of CFP-actin (72 hours) and imaging of CFP-actin bundles over many hours (supplementary material Fig. S1) demonstrated that CFP-actin expression did not affect cell viability. This proved that the gene was producing a fully functional mRNA and protein, and we could then proceed to analyze the mRNA in both nuclear and cytoplasmic compartments.

Kinetics of mRNA transcriptional induction

Examination of mRNA transcription from the integrated gene by fluorescence in situ hybridization (RNA-FISH), with a fluorescent probe for the MS2 region, detected the nuclear transcription site in cells induced with dox for 1-3 hours (Fig. 2A). At later times after

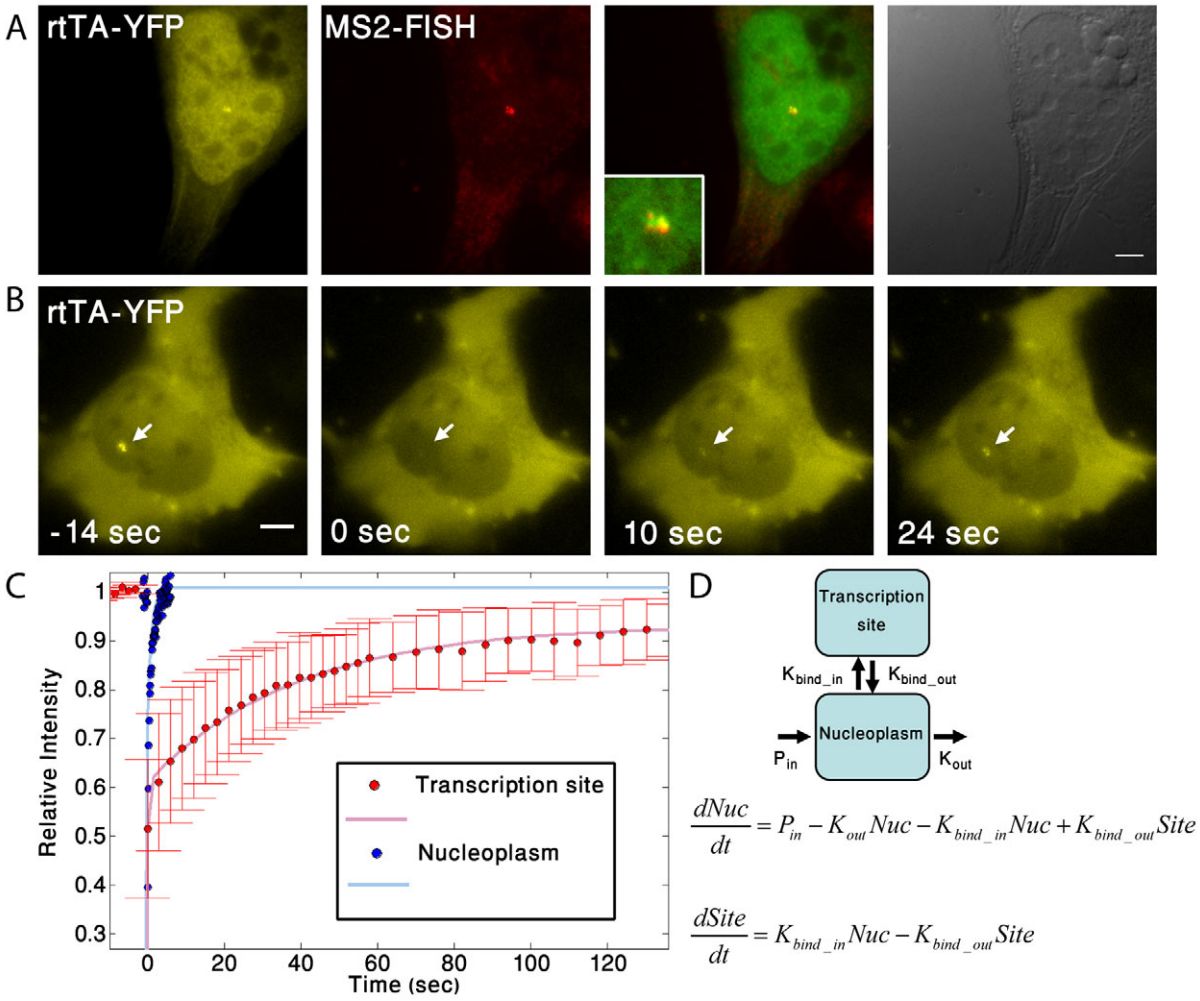

Fig. 3. The dynamics of rtTA association with the active gene. (**A**) rtTA-YFP (yellow) is recruited to actively transcribing sites (red, MS2 FISH). The box in merge shows the transcription site. (**B**) Frames from a FRAP experiment showing the rtTA-YFP signal at the transcription site before and after photobleaching (arrow). (**C**) FRAP recovery curves of rtTA-YFP at the transcription site (red dots and line fit) and freely diffusing in the nucleoplasm (blue dots and line fit). (**D**) Scheme of the model and differential equations describing the entrance and exit kinetics of rtTA-YFP molecules at the transcription site. Scale bars: 5 μm.

dox induction, a strong cytoplasmic β-actin–MS2 mRNA signal was observed, indicating nucleo-cytoplasmic transport of the mRNA. The recruitment of endogenous RNA polymerase II (RNA Pol II) to the active transcription sites was detected by immunofluorescence of the elongating form of RNA Pol II using the H14 antibody (Fig. 2B). Interestingly, the LacI signal marking the non-coding region of the genes (*lacO*) was found in the center of the gene locus and was surrounded by a distinctly separate signal from the polymerase and the nascent mRNAs (Fig. 2B,C). We further confirmed that the actively transcribing sequences were organized around the *lacO* sequences on the basis of the similar presence of the ASF/SF2 splicing factor at the actively transcribing gene locus (Fig. 2D). The recruitment of the transcriptional activator rtTA to active genes was detected at the transcription sites in cells expressing rtTA-YFP; this signal also surrounded the LacI signal (Fig. 2E). This analysis demonstrated the unique organization of the transcription site, with the non-coding regions of the gene located in the inner part of the locus and the transcribing portions of the gene facing outwards probably in order to contact the nucleoplasmic environment and the transcriptional machinery recruited to the gene.

To examine the binding kinetics of the rtTA transcription factor to the active promoter (Fig. 3A), we photobleached the rtTA-YFP signal at the transcription site and followed the recovery of fluorescence over time (fluorescence recovery after photobleaching, FRAP) (Fig. 3B; Fig 3C, red dots). In comparison, we photobleached the freely diffusing protein found in the nucleoplasm; this population showed very rapid recovery kinetics typical of freely diffusing proteins (diffusion coefficient (D)=~8 μm^2/second; Fig. 3C, blue dots). To calculate the residence time of the transcription factor on the promoter, we modeled the data using a simple two-phase mathematical model consisting of ordinary differential equations (ODEs) (Fig. 3D). We could clearly identify the two protein populations in the recovery curve (Fig. 3C, red dots): the fast freely diffusing population and the proteins binding at the transcription site. Diffusion of free rtTA-YFP was very fast compared with the bound population and with the timescale of the FRAP measurement. Therefore, we could measure the binding time of the protein (Sprague et al. 2004). The model shows that 4.7% of the rtTA-YFP protein population attached to the promoter region and remained there for 40 seconds on average. These dynamics showed the transient nature of rtTA transcription factor binding to the *tet* operator (*tetO*) promoter region.

We next were interested in measuring the kinetics of the β-actin–*MS2* mRNA at the site of transcription in single living cells. We tagged the mRNAs with YFP-MS2(-nuclear localization signal; NLS) protein (Fig. 1A). Because each MS2 stem-loop in the mRNA binds a dimer of YFP-MS2 proteins, each mRNA is coated with more than 30 YFPs (Fusco et al., 2003). This provided a good signal-to-noise ratio for the mRNP signal above the YFP-MS2 diffuse nucleoplasmic background. We followed the timing of transcription induction and mRNA synthesis in long 4D time-lapse movies (imaged in 3D every 5 minutes, 5 minutes after dox induction) and could detect the induction of mRNA synthesis at the transcription site 20 minutes after dox addition to the medium (Fig. 4A; supplementary material Movie 1). There was a gradual increase in the YFP-MS2 signal at the transcription site for another 40 minutes, implying that the full induction of the gene array occurred gradually.

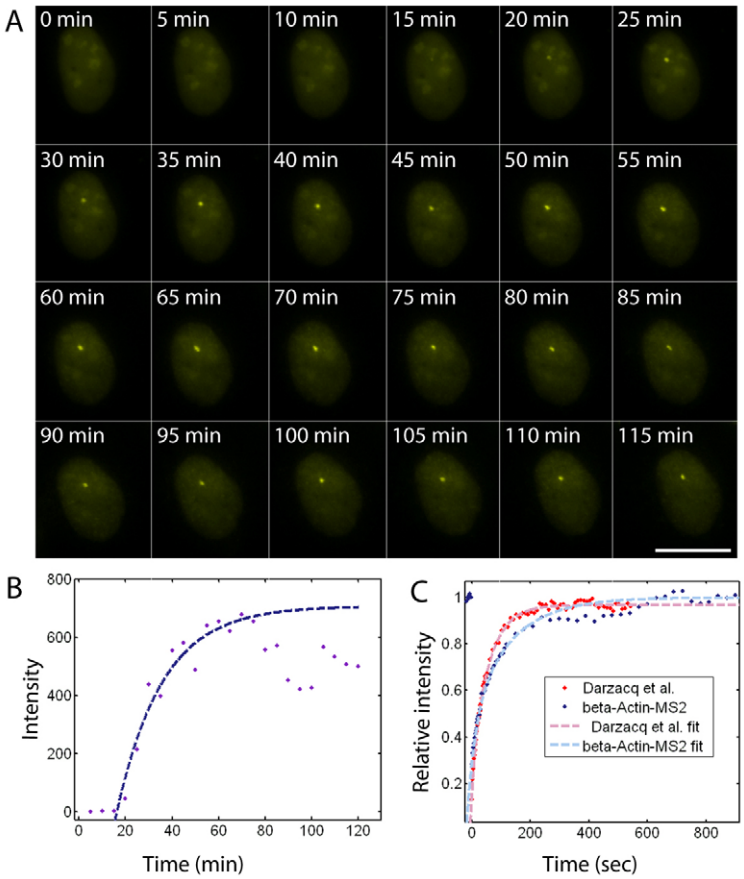

Fig. 4. Kinetics of mRNA transcription. (**A**) Cells expressing YFP-MS2-NLS were imaged for 115 minutes [every 5 minutes, starting 5 minutes after dox induction (t=0)]. The induction of the transcription site was followed. Scale bar: 20 μm. (See also supplementary material Movie 1.) (**B**) The signal at the transcription site in A was quantified over time (dots). There is an initial linear increase after the induction of transcription that slows over time (following the form $Ae^{-Bt}+C$), showing the time required to reach a steady state. The fit (line) shows a deviation after 80 minutes. (**C**) Active transcription sites were photobleached and the recovery of fluorescence was recorded (supplementary material Movie 3). The recovery is proportional to the polymerase rates. The FRAP recovery curves and fits of photobleached transcription sites in the β-actin–MS2 cells (blue) are compared with those of a similar experiment on another gene (red) (Darzacq et al., 2007).

The transcription site signal intensity reached a plateau ~60 minutes after induction, indicative of reaching a steady state involving the transcription of new mRNAs and the release of mature mRNPs. After another ~20 minutes, a gradual decrease in site signal intensity was observed (Fig. 4B). Overall, we found that a pulse of transcription induction requires at least an hour to reach maximal activity, and that these kinetics are characterized by a gradual increase and decrease in transcriptional activity.

Kinetics of transcriptional induction following cell division

Because the YFP–MS2-transfected cells continued to divide in culture, we found this cell system useful for examining whether there is synchronization of transcriptional induction in the two daughter cells appearing after mitosis. We performed long-term 4D imaging of cells in a dox-induced population to identify cells undergoing mitosis. We then examined the time-lapse movies in which mitosis occurred and looked for cells in which the CFP-actin gene was induced after cell division. We found that each daughter cell began transcribing at a different time point following division. Even relatively large lag times of ~2 hours between transcriptional activation times could be found. We therefore conclude that daughter cells after mitosis are not synchronized with respect to the transcriptional activation of the gene array, even though the cells are closely situated in space and are likely to be exposed to the same doxycycline activating signals (Fig. 5; supplementary material Movie 2).

Kinetics of mRNA elongation

To directly probe RNA Pol II elongation kinetics on the gene array in vivo, we used a photobleaching approach previously devised for examining transcriptional kinetics on an integrated gene array (Boireau et al., 2007; Darzacq et al., 2007). We photobleached the labeled mRNA signal being transcribed at the active transcription sites using FRAP and followed the recovery of the YFP-MS2 signal over time. This method enables the measurement of transcription rates, because the recovery rates of the fluorescent signal reflect the speed of new mRNA production and are therefore proportional to RNA Pol II elongation rates. We used a 3D FRAP system in which rapid imaging allowed the acquisition of the full 3D nuclear volume during FRAP recovery recordings. Thereby, no signal was lost during the experiments. We preformed FRAP experiments on the active transcription sites (supplementary material Movie 3), collected 3D data and calculated the recovery curves (Fig. 4C). The curve fits were compared to a kinetic model describing elongation that is based on differential equations (Darzacq et al., 2007). The initial step of the model (entry point) is elongation, namely the process responsible for synthesizing new MS2-binding sites. The end step (exit point) is mRNA release into the nucleoplasm. The model is based on the recovery curves, which consist of two kinetically resolved components, one fast and one slower. The fast component refers to elongation, whereas the slower component was modeled as polymerase pausing during elongation. The two polymerase states were modeled as elongation with a stochastic transition to pausing. We optimized the differential equations from this model, which yielded an elongation speed of 3.3 kb/minute with a stochastic transition to a slower synthesis rate (pausing for a cumulative time of 2.5 minutes). Modeling showed that this transition from elongation to pausing affected only 4% of the polymerases that entered elongation. Indeed, a recent analysis of elongation kinetics for a variety of genes using microarray and reverse transcriptase (RT)-

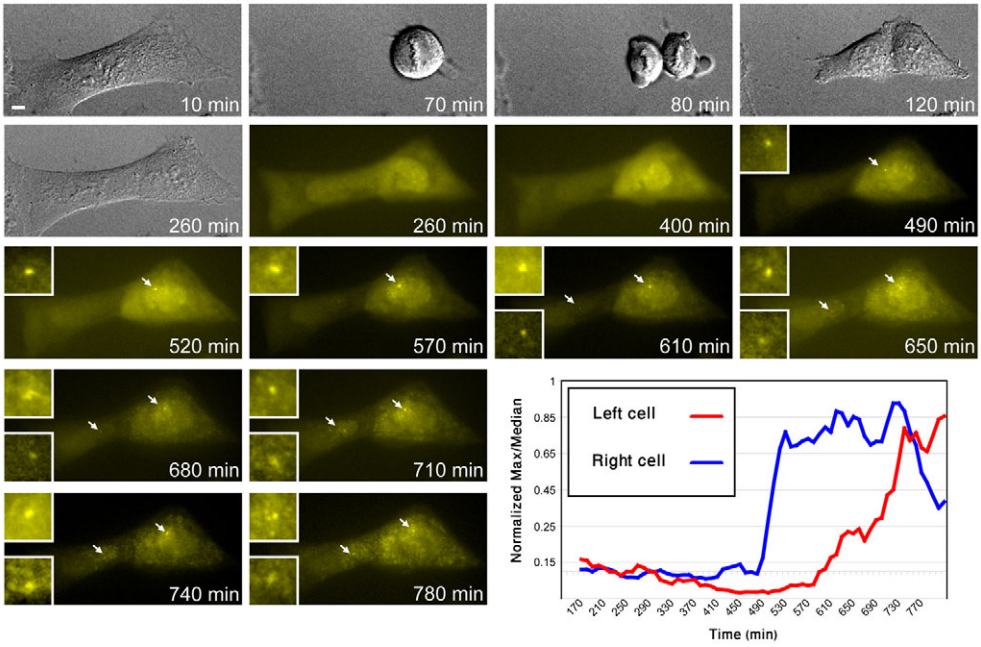

Fig. 5. **Transcription induction in daughter cells is not synchronized.** DIC images (top row) show the division of the imaged cell (dox was given at *t*=0). Fluorescence images of the YFP–MS2-expressing daughter cells are shown from 260 minutes after dox induction (sum projection of three slices centered on the plane in focus) (supplementary material Movie 2). Arrows and boxes highlight the activated transcription sites. For each nucleus, we measured the maximum (active transcription site) and median (free YFP-MS2) pixel value and plotted their ratio over time in both cells. For presentation and noise reduction, data were smoothed by averaging every four time points, beginning from the time point after cell division. Left daughter cell – red, right daughter cell – blue line. Scale bar: 5 μm.

PCR techniques (Singh and Padgett, 2009; Wada et al., 2009) fits well with the measured polymerase elongation rates for this β-actin gene, showing that the polymerase kinetics are potentially faster than previously determined (Darzacq et al., 2007).

Kinetics of mRNA accumulation in the cytoplasm

In the above experiments, mRNPs were seen moving throughout the nucleoplasm. To improve signal detection of the β-actin–MS2 mRNPs in vivo, we generated a modified version of the YFP-MS2 protein that imitated the nucleocytoplasmic shuttling properties of proteins that normally coat mRNAs. The addition of a nuclear export sequence (NES) to the protein balanced out the effect of the NLS and, at moderate expression levels, the NES-YFP-MS2-NLS construct provided a low background throughout the whole cell (under non-induced conditions) (supplementary material Fig. S2). This enabled longer imaging sessions because exposure times could be reduced. We also verified that this version did not affect the above measured kinetics at the transcription site. We could follow the gene (RFP-LacI), the mRNA (YFP-MS2) and the protein product (CFP-actin), as the mRNAs and protein accumulated in the cells for many hours (supplementary material Fig. S3 and Movie 4). The mRNPs first accumulated in the nucleoplasm and later on in the cytoplasm, as expected, detectable in a 10-30 minute time frame from the initiation of transcription (Fig. 6A; supplementary material Movie 5). We quantified the increase in cytoplasmic mRNPs in comparison to the nuclear population by counting the number of mRNPs in the 3D volumes of the cell acquired in supplementary material Movie 5. A steady level of nuclear mRNPs (~200) was found to be maintained throughout the period of gene activation compared with the time-dependent increase in the cytoplasm (Fig. 6B). In this particular cell, with a large well-spread cytoplasm, the gradual diffusion of mRNAs from the nuclear periphery and outwards was clearly observed (Fig. 6C). At later times, the emptying out of the nucleus was detected and, with the shutdown of the transcription site, the cytoplasmic mRNP population also began to decrease. Our measurements showed that general mRNA translocation rates were effectively transferring the pool of nuclear mRNAs during ongoing transcription. This was seen as a constant flux of mRNAs into the cytoplasm and their dispersal in the whole cytoplasmic volume, without retention in the nucleus.

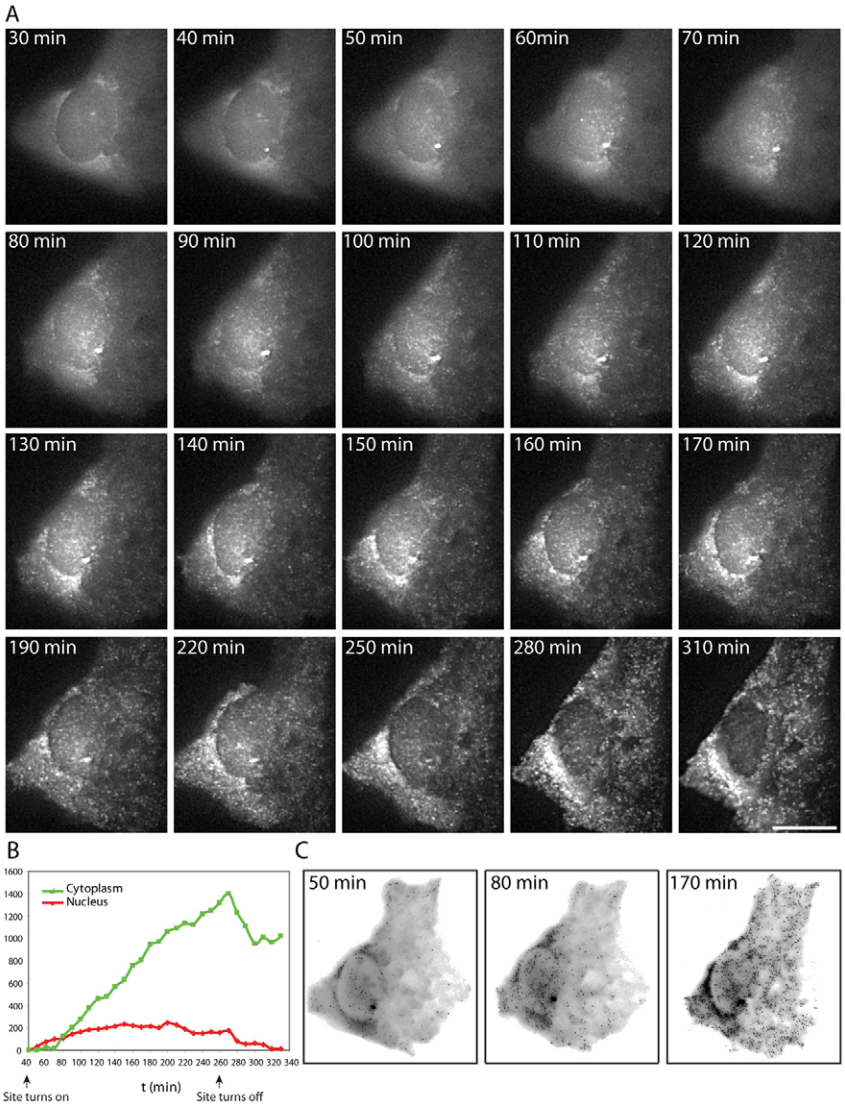

Fig. 6. Kinetics of mRNA transport. (**A**) Cells expressing NES-YFP-MS2-NLS showed transcription site induction followed by the appearance of tagged mRNPs (original frames of supplementary material Movie 5 were deconvolved to enhance the mRNP signal). Cells were imaged for a total of 5.5 hours, every 10 minutes (dox induction at *t*=0 minutes). An active transcription site was seen at *t*=40 minutes. Approximately 10 minutes later, transcripts were detected in the nucleoplasm (50 minutes) and ~10 minutes after that in the cytoplasm (60 minutes). Scale bar: 20 μm. (**B**) Graph representing the number of mRNPs counted in the 3D volumes of the nucleus (red) and the cytoplasm (green) throughout each frame of the movie. The plot begins at *t*=40 minutes, the initial time point of transcription site activation. The site turns off at 260 minutes. (**C**) Three frames (*t*=50, 80, 170 minutes) representing the increase in mRNP levels in the cell over time and the distribution of mRNPs towards the periphery of the cytoplasm. These three frames are projections of all the mRNPs in the 3D volume of the cell, presented in one frame. Therefore, the mRNA signal is pronounced in the region surrounding the nucleus, where the cytoplasmic volume is large.

The dynamics of cytoplasmic mRNA targeting

We then examined the distribution of the mRNAs in the cytoplasm. The bulk of mRNA transcripts in the cytoplasm move by diffusion (Fusco et al., 2003) and typically many are found in the vicinity of the nuclear periphery. A certain portion of the mRNA, as in the case of β-actin mRNA, can also attach to the actin cytoskeleton and localize. RNA-FISH with specific probes that differentiate between the human and chicken β-actin mRNAs in our cell system showed the orderly decoration of some of the cytoplasmic β-actin bundles (marked with CFP-actin) with mRNA molecules (Fig. 7A). This could also be observed for a portion of the YFP–MS2-labeled mRNPs (supplementary material Fig. S4). Spatially separated cytoplasmic signals were detected for both of the mRNAs transcribed from either the endogenous or integrated β-actin genes (Fig. 7A), demonstrating that these mRNAs were transcribed and transported as separate mRNP entities.

We then examined β-actin mRNA localization in these cells using RNA-FISH. The human osteosarcoma U2OS cell line is highly metastatic (Hotulainen and Lappalainen, 2006; Khyrul et al., 2004), is particularly motile in culture when plated as single cells and exhibits a polarized shape upon movement (see supplementary material Fig. S5A and Movie 6). In addition to the motility of the leading edge of the cell, U2OS cells also produce prominent retraction fibers during movement (supplementary material Fig. S5B). β-actin mRNA localization is enhanced after release from serum starvation (Latham et al., 1994). We examined the endogenous human β-actin mRNA cytoplasmic distribution in U2OS cells following release from serum starvation. Under conditions of serum starvation, β-actin mRNAs were predominantly found at the nuclear periphery and not at the leading edge of the cell, even when the cells were well spread (Fig. 7B). When serum was added to the cells, we detected cells with β-actin mRNA now localized at the moving edge of the cell (Fig. 7B). Within 30 minutes of release from serum starvation, the percentage of cells with localized mRNA increased from 9±0.4% to 28±4.6% (Fig. 7C). Previous measurements in primary chick embryonic fibroblasts found an increase in the localization of β-actin mRNA from 12.5% to 20-25% of the cells after 10 minutes of serum induction (Latham et al., 1994). The β-actin mRNA was also found to concentrate at the cell periphery during the process of cell adherence to the substrate (supplementary material Fig. S5C). The endogenous human homologue of ZBP1 (termed IMP1) (Vikesaa et al., 2006; Yisraeli, 2005) was also found at the leading edge of the cells (Fig. S5D), as well as RFP-ZBP1 in live-cell experiments of a moving edge of a cell (supplementary material Fig. S6 and Movie 7) and during adherence (supplementary material Fig. S7 and Movie 8). Following this analysis, we proceeded to use these cells for the analysis of cytoplasmic β-actin mRNA dynamics.

We first examined the localization of β-actin–MS2 mRNAs by FISH. In serum-starved cells, most of the mRNA was found at the nuclear periphery and no significant portion of the cellular mRNA could be detected at the cytoplasmic edge (Fig. 8A). However, after 20-30 minutes of serum induction, β-actin–MS2 mRNAs could be detected at the leading edge of cells and also decorating some of the CFP-actin bundles (Fig. 8A). In addition, β-actin–MS2 mRNA had a similar distribution to the localized human mRNA in adhering cells (Fig. 8B). These experiments indicate that the zipcode elements in the mRNA are sufficient for mRNA targeting to the leading edge across species. We then examined localization in live-cell experiments in which the β-actin–MS2 mRNAs were tagged with YFP-MS2. We first imaged cells without any mRNP signal at their leading edges. Serum was added during imaging and the gradual localization of β-actin–MS2 mRNPs in cytoplasmic protrusions 20-30 minutes after serum addition was observed, showing a twofold increase in the level of tagged transcripts in the cytoplasmic periphery (Fig. 9 and supplementary material Movie 9). Comparing the time frames of cytoplasmic

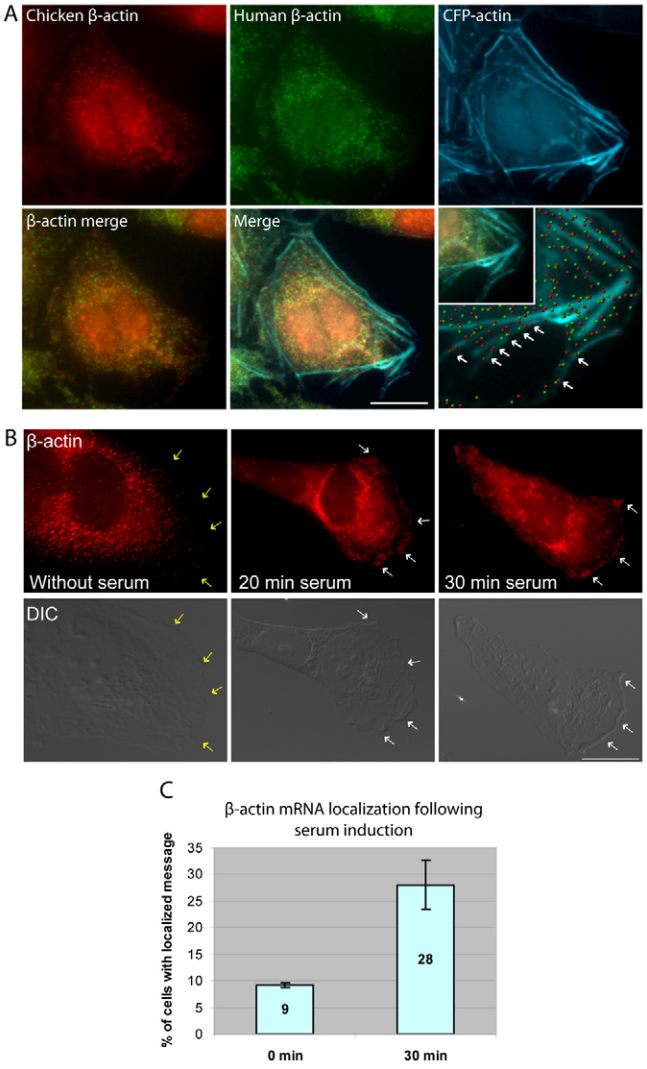

Fig. 7. Cytoplasmic distribution of β-actin mRNAs. (**A**) RNA-FISH with a Cy3-MS2 probe against chicken β-actin–MS2 mRNA (red) and a Cy5–β-actin probe against human β-actin mRNA (green) showed spatial separation between the mRNAs. Both mRNA species were found to decorate CFP-actin bundles. In the enlarged area (bottom right), mRNPs (red and green balls) are situated along some of the CFP-actin bundles. Scale bar: 10 μm. (**B**) Human β-actin mRNA is mostly centrally localized in the cytoplasm of untreated U2OS cells, as seen by RNA-FISH (Cy3–β-actin probe), even when the cell is well spread (yellow arrows show cell edges). Following serum induction (20 or 30 minutes) of serum-starved cells, human β-actin mRNA is detected at the leading edge (white arrows). Scale bar: 20 μm. (**C**) 200 cells with prominent leading edges were analyzed by DIC with a Cy3 probe and counted at each time point. Positively localizing cells had a strong endogenous mRNA signal at the leading edge, in comparison to cells devoid of signal in this region. The percentage of cells with localized mRNA following serum induction is plotted.

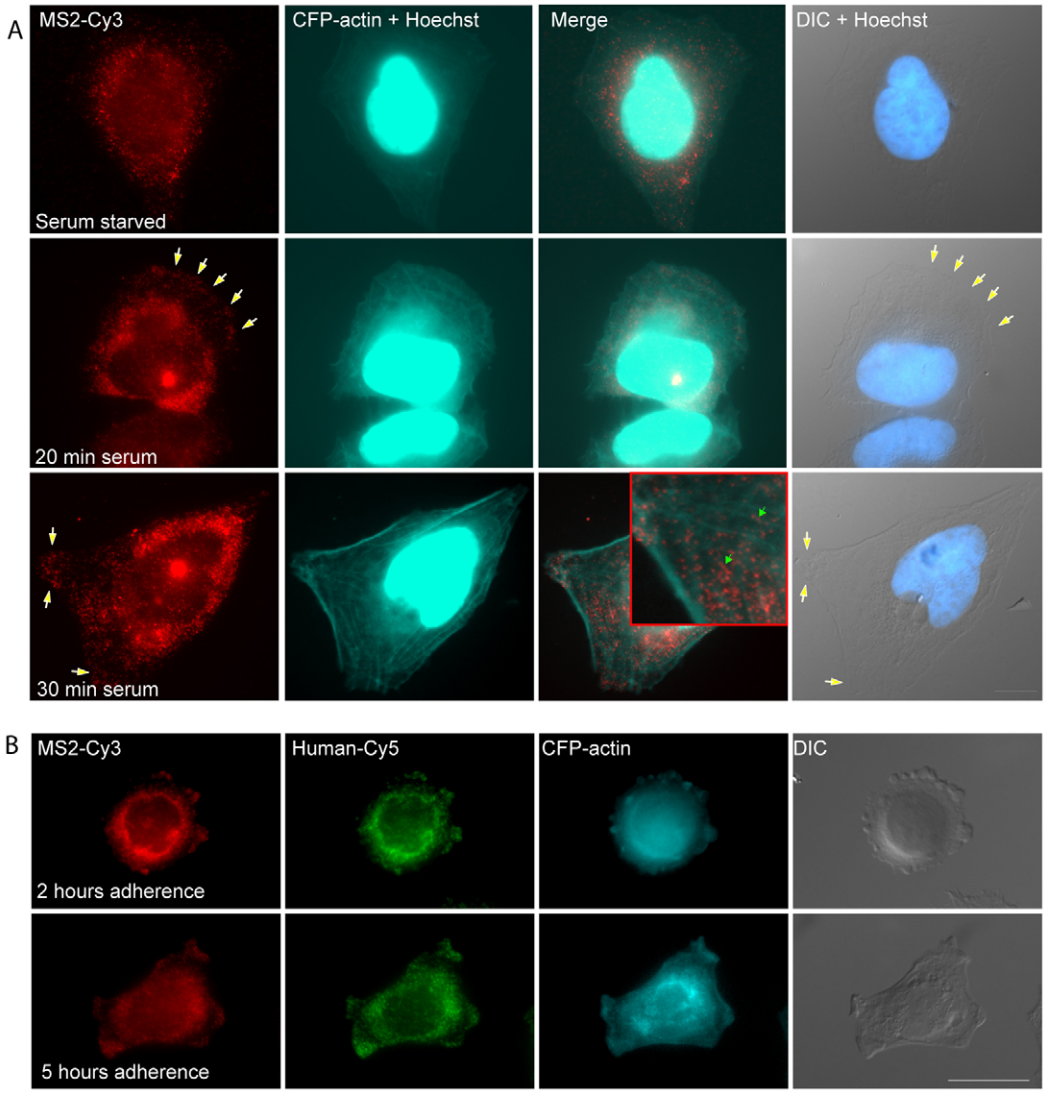

Fig. 8. Localization of chicken β-actin–MS2 mRNA. (**A**) RNA-FISH with a Cy3-MS2 probe against the β-actin–MS2 mRNA showed that the transcripts were centrally distributed in serum-starved cells (top) and localized to the leading edge after 20-30 minutes of serum stimulation (middle and bottom, yellow arrows). Cells were imaged in the CFP channel for CFP-actin. Hoechst nuclear staining was also detected in this channel as a strong signal in the center of the cell. The enlarged inset shows a series of mRNAs decorating CFP-actin fibers (green arrows). (**B**) Following overnight dox induction, adhering cells were seeded and dox was added one hour later. Cells were fixed 2 or 5 hours after plating. RNA-FISH with a Cy3-MS2 probe against the β-actin–MS2 mRNA (red) and a Cy5–β-actin probe against the human β-actin mRNA (green) showed that the mRNAs had a similar pattern of localization to the cell periphery. Scale bars: 10 μm.

localization (~20 minutes) to the above-measured kinetics of transcription induction and translocation to the cytoplasm (10-30 minutes) suggested that the initial localizing population of mRNAs must be derived from an existing population of cytoplasmic mRNAs rather than from the newly transcribed mRNAs. To examine these kinetics more closely, we analyzed the diffusion properties of the β-actin mRNPs in both compartments.

Temporal dynamics of nucleoplasmic and cytoplasmic mRNPs

We compared the diffusional properties of β-actin–MS2 in both nuclear and cytoplasmic compartments. We tracked the movement of single YFP–MS2-labeled mRNPs in the time-lapse movies using single-particle tracking (SPT) (Fig. 10A,B). The diffusion coefficients were calculated according to the mean square displacement (MSD) equation, as previously described (Shav-Tal et al., 2004). The diffusion of the mRNPs in the nucleoplasm was slightly slower [D=0.024 μm^2/second (mean, n=34)] than movement in the cytoplasm [D=0.035 μm^2/second (mean, n=58)] (Fig. 10C), probably due to differences in compartment crowding. Diffusional movement of mRNPs can be one of two major types – simple diffusion or constrained diffusion that is hindered by nuclear or cytoplasmic structures. There was less constrained diffusional movement in the cytoplasm (45.6%) compared to the nucleoplasm (70.6%), attributed to the dense structure of nuclear chromatin. The meaning of the nucleoplasmic mRNP diffusion rates is that the kinetics of mRNP transport into the cytoplasm should take place in the 10 minute range (see example in Discussion). We also measured the diffusion rates of cytoplasmic mRNPs using FRAP, whereby a population of mRNPs was

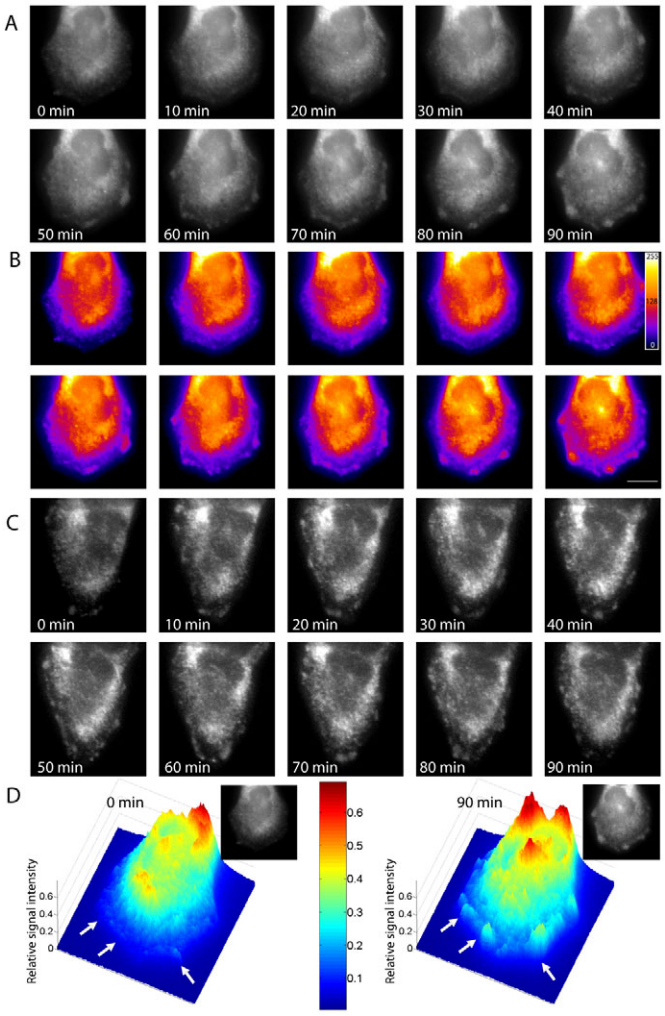

Fig. 9. Localization of YFP–MS2-labeled mRNPs in living cells. Cells expressing NES-YFP-MS2-NLS were induced with dox overnight. After raising the FCS levels to 20%, cells were imaged every 10 minutes. (**A**) The appearance of the β-actin–MS2 mRNA at the cell front was observed after addition of serum. (**B**) The same cell as in A with a different color representation, showing the appearance of mRNPs at the leading edge (supplementary material Movie 9). The color scale indicates levels of image intensity from 0-255. (**C**) Example of another cell showing mRNP localization. Scale bar: 5 μm. (**D**) 3D representation of the signal of YFP–MS2-labeled β-actin–MS2 mRNA in A at times 0 and 90 minutes, showing the increase in peripheral localization. The relative increase in signal intensity is shown on the color scale.

photobleached and then the return of fluorescent mRNPs into the bleached region was monitored (Fig. 10D). This analysis showed faster kinetics compared to the SPT measurements (D=0.13 μm^2/second), probably due to the tendency to detect slower particles by SPT. The diffusional kinetics of cytoplasmic mRNPs were not affected when the cytoskeleton was disrupted using nocodazole (microtubule disassembly) or cytochalasin D (actin disassembly) (Fig. 10E). These experiments imply that the majority of the mRNP population in both compartments is moving by diffusion and that this suffices for the availability of mRNP interactions with the translation machinery throughout the cytoplasm.

Discussion

In this study, we set out to follow the kinetics of the main events in the life cycle of an mRNA until it reaches a cytoplasmic destination. No study has followed and quantified the full cellular pathway of an mRNA, in particular a functional mRNA that plays an important biological role. We examined the different phases in the mRNP life cycle and obtained the transcription rates of Pol II, the kinetics of transcription factor association with the gene, the dynamics of mRNP transport through the nucleoplasm and the cytoplasm, and the kinetics of cytoplasmic localization.

β-actin was the gene of choice. It is an essential housekeeping gene that has a distinct mRNA and protein distribution pattern. β-actin mRNA localization has been suggested to replenish the high levels of β-actin protein required at the moving edge of the cell for polymerization and lamellipod translocation in chicken embryo fibroblasts (Condeelis and Singer, 2005). We used the chicken β-actin-coding region and its 3′-UTR because this species is the best characterized. The mRNA behaved in human osteosarcoma cells as it does in chicken fibroblasts; hence, the signals directing localization and translational regulation were recognized in these cells, most probably because of the high conservation of the *trans*-acting zipcode-binding protein (Huttelmaier et al., 2005).

By studying the dynamics of β-actin mRNA in vivo, we could ask whether the serum response of the β-actin gene, in which both transcription and mRNA localization are induced, involves two interconnected steps or independent processes. RNA-FISH studies have shown that serum induction of β-actin transcription takes 5-10 minutes (Femino et al., 1998). We show here that the translocation of significant amounts of β-actin mRNA into the cytoplasm occurs within the 10-20 minute range, whereas localization to the leading edge occurs in parallel during the same time frame. Translocation of β-actin mRNA towards the moving edge of the cell has been observed to begin within 5 minutes of serum stimulation (Latham et al., 1994). Altogether, this means that β-actin mRNA localization depends initially on an existing cytoplasmic β-actin mRNA pool rather than on the newly synthesized mRNAs, because these would take a while to reach the cytoplasm.

The nucleoplasmic phase of an mRNA should be as brief as possible. This part of the mRNP journey is composed of a transcription phase and a translocation phase. We first examined the transcriptional process. Transcriptional induction of the gene array occurred gradually and later showed a decrease in transcription site intensity after reaching a plateau of activity. The latter has been observed in a number of other transcription systems (Archer et al., 1994; Femino et al., 1998; Muller et al., 2001), which might be indicative of an inhibitory effect of the high levels of transcripts on the transcription site. The structure of the transcription site during activation was of interest. The non-coding *lacO* repeats were found situated in the center of the gene locus, whereas the transcribing sequences were externally positioned, as was seen from the accumulation of the polymerase, transcription factor, splicing factor and mRNAs in a flower-shaped structure surrounding the non-coding region. This structure is reminiscent of the suggested clustering of active genes into dedicated transcription factories, where they are efficiently transcribed on account of the enrichment of the necessary factors in the factory region (Iborra et al., 1996; Pombo et al., 2000; Sutherland and Bickmore, 2009).

Using a photobleaching approach, we measured a rate of 3.3 kb/minute for polymerase elongation. These kinetic properties were similar to the rates (up to 4.3 kb/minute) measured for a similar

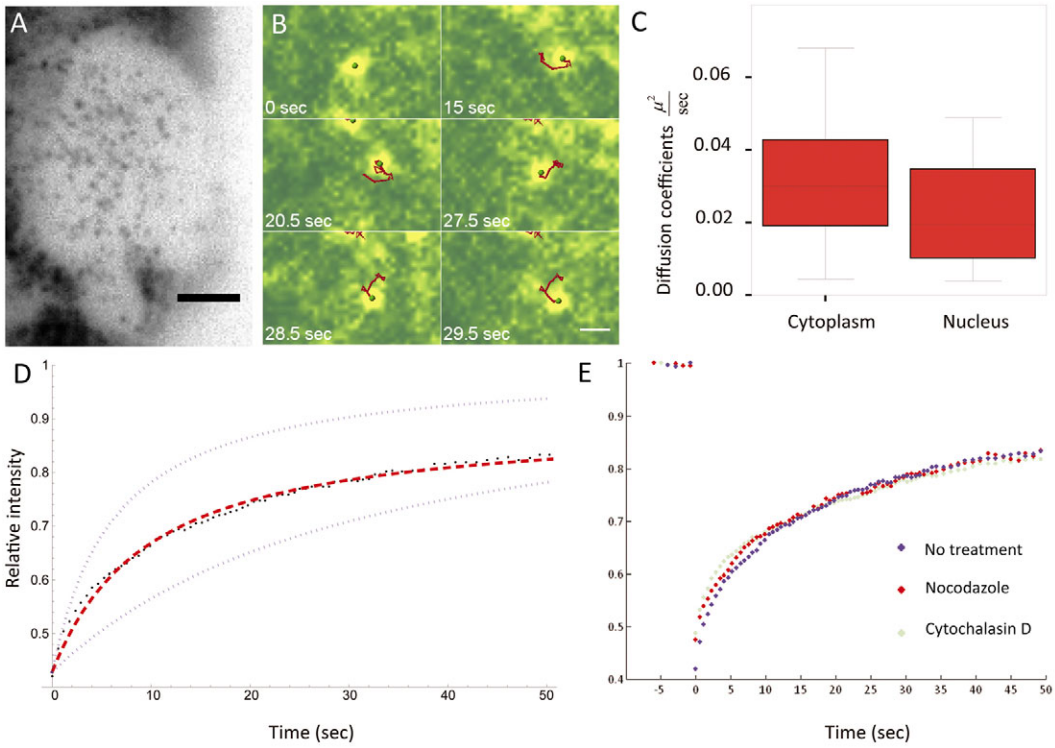

Fig. 10. Diffusion kinetics of nuclear versus cytoplasmic mRNPs. (**A**) β-actin–MS2-labeled mRNPs were detected either in the nucleoplasm (nucleus with mRNPs shown in a color-inverted representation) or in the cytoplasm of dox-induced cells. Scale bar: 5 μm. (**B**) mRNPs (pseudo-colored yellow, center of mass in green) were tracked from frame to frame (red track). Scale bar: 0.5 μm. (**C**) Diffusion coefficients for nuclear and cytoplasmic mRNPs were calculated. (**D**) Cytoplasmic mRNPs (n=17 cells) were photobleached (FRAP) in an ROI and the diffusion coefficient was calculated from the fit of the FRAP curve (D=0.13 μm^2/second). Dotted lines show the curve behavior if D=0.22 μm^2/second (top) or D=0.09 μm^2/second (bottom). (**E**) FRAP recovery rates were similar in untreated (blue dots) cells versus cells treated with nocodazole (red dots, n=19 cells) or cytochalasin D (grey dots, n=22).

gene construct (Darzacq et al., 2007; Janicki et al., 2004). Although previous measurements have typically found transcription rates of 1-2 kb/minute, two recent studies using molecular approaches have strengthened the notion that Pol II rates are much faster, ranging between 3 and 4 kb/minute (Singh and Padgett, 2009; Wada et al., 2009). The 3.6 kb mouse β-actin gene would therefore require a 1-2 minute period for β-actin mRNA synthesis when elongation is running at rates of over 3 kb/minute. Because the serum response of the murine β-actin gene requires between 5 and 10 minutes before the first mRNAs are completed (Femino et al., 1998), this would suggest that the assembly of a pre-initiation complex containing the appropriate transcription factors and the polymerase is the limiting factor in the process. This has been implied by other studies (Darzacq et al., 2007; Dundr et al., 2002; Juven-Gershon et al., 2008).

The measured kinetics of rtTA transactivator interaction with the promoter was 40 seconds. Indeed, several studies have quantitatively measured the kinetics of transcription factor binding to promoters and have demonstrated a wide variety of transient interactions of up to 100 seconds (recently reviewed in Hager et al., 2009). The scenario of promoter-factor binding emerging from these studies is that a combination of stochastic interactions with the promoter occasionally leads to assembly of fruitful interactions that culminate in transcription. We could demonstrate this by comparing the transcription induction kinetics of the newly formed daughter cells after cell division. Interestingly, there was no synchronization in the timing of transcriptional activation of the gene array between daughter cells after mitosis. In fact, a significant interval of more than 2 hours between activation events was seen, suggesting that the cells were autonomous in their transcriptional activation decisions. This would depend on the relative abundance of available transactivating factors and the probability of obtaining fruitful interactions on the promoter in each cell independently.

To date, no directional translocation system has been detected for nuclear mRNA transport. Instead, diffusion has been observed to be the mechanism used by cells for moving mRNAs into the cytoplasm (Bassell et al., 1999; Politz and Pederson, 2000; Shav-Tal and Gruenbaum, 2009). The transport of β-actin mRNA transcripts agrees with previous calculations of diffusion coefficients measured for diffusing mRNPs in the nucleoplasm (Shav-Tal et al., 2004). A simulation of nuclear mRNPs moving by random diffusion (Braga et al., 2004) [D=~0.04 μm^2/second (Shav-Tal et al., 2004)] in a ~8 μm diameter nucleus that contains 2000 randomly scattered pores has shown that the average time required for an mRNP particle to reach a nuclear pore would be approximately 6 minutes (Braga et al., 2007; Calapez et al., 2002). Overall, these studies suggest that mRNA translocation into the cytoplasm occurs in accord with the biological constraints necessary for a protein synthesis response within minutes.

The diffusion properties of nuclear and cytoplasmic single mRNPs were separately followed in three previous studies: a cytoplasmic mRNP containing the LacZ-coding region with an MS2 3′-UTR (Fusco et al., 2003), a nucleoplasmic mRNP containing the CFP-coding region with an MS2 3′-UTR (Shav-Tal

et al., 2004) and a nucleoplasmic mRNP containing 96 repeats of a 50-nucleotide region that contains binding sites for molecular beacons (Tyagi and Alsmadi, 2004; Vargas et al., 2005). Although the diffusion of mRNA in the nucleoplasm occurs rather slowly, probably due to the chromatin constraints that the mRNAs encounter en route to the nuclear envelope, the diffusion coefficients in the cytoplasm are typically faster. Fusco et al. measured diffusion coefficients for cytoplasmic mRNAs carrying the β-actin 3′-UTR in the range 0.013-0.045 μm^2/second for long-range diffusion and 0.1 μm^2/second for short-range diffusion (Fusco et al., 2003). We obtained measurements for the same mRNA in both cellular compartments (nucleoplasm 0.024 μm^2/second; cytoplasm SPT 0.035 μm^2/second, FRAP 0.13 μm^2/second). Our data emphasize that the prevalent motion of cytoplasmic mRNAs is diffusion and that cytoplasmic diffusion rates are not affected by the existence of an intact cytoskeleton.

Directional dissemination of mRNA from the site of transcription to the cytoplasm is based mostly on random movement. When long transport distances must be overcome, such as in neuronal cells (Kiebler and Bassell, 2006), the cell is required to invest energy to localize specific mRNAs to regions of cell specialization. The cell has evolved a general, simple and energy-conserving mechanism for transport of mRNA from the site of transcription to the site of translation. The stochastic nature of mRNA expression means that not all mRNAs and not all cells are in the same state at any one moment, and that regulation of protein synthesis will rely on intrinsic (diffusion) and extrinsic (signaling) factors exerted through the spatial and temporal dimensions.

Materials and Methods

Plasmids

The p3216PECactMS2act3UTRβ plasmid [32 *lacO* units, 16 TRE units, the cytomegalovirus (CMV) minimal promoter (P), CFP–chicken-β-actin (Cact), 24 MS2 repeats (MS2), chicken β-actin 3′-UTR (act3UTR) and a rabbit β-globin intron-exon module (β)] was constructed from the previously described p3216PECMS2β plasmid (Janicki et al., 2004) by replacing the CFP-SKL-24MS2 fragment with a CFP–actin–24MS2–3′-UTR fragment using *Age*I and *Apa*I. RFP-ZBP1 was generated by cloning the ZBP1 gene from a GFP-ZBP1 plasmid into RFP-C1 using *Xho*I and *Hin*dIII. To construct NES-YFP-MS2-NLS, the minimal LPPLERLTL HIV-REV-NES coding sequence was synthesized as an adaptor containing 5′-*Xba*I and 3′-*Nco*I restriction sequences, and cloned 5′ to the original YFP-MS2-NLS. rtTA-YFP was previously described (Janicki et al., 2004).

Cell culture

Human U2OS and U2OS Tet-On cells were maintained in low-glucose DMEM (Biological Industries, Israel) containing 10% FBS (HyClone). Cells were transfected by electroporation as previously described (Shav-Tal et al., 2004). U2OS Tet-On stable lines were stably cotransfected with the p3216PECactMS2act3UTRβ construct (5 or 10 μg) and a puromycin-resistance plasmid (1 μg). Puromycin-resistant (100 μg/ml, Sigma) clones were screened for CFP-actin expression following overnight induction with 1.5 μg/ml doxycycline (Sigma). Single locus integration was verified by transient expression of RFP-LacI. Clone 43 was selected for further use because it harbors a small integration site. For serum-starvation experiments, cells were maintained in medium without serum overnight and then induced with 10% serum for the indicated times. For cytoskeleton disassembly, cells were treated with 600 nM nocodazole (30 minutes) or 1.25 μg/ml cytochalasin D (1 hour).

Western blotting

SDS-PAGE and western blotting were performed as previously described (Aizer et al., 2008). Primary antibodies were used as follows: horseradish peroxidase (HRP)-conjugated anti-β-actin (Santa Cruz), anti-α-tubulin and anti-GFP (Covance). The secondary antibody used was HRP-conjugated goat anti-mouse IgG (Sigma).

Immunofluorescence and RNA-FISH

Immunofluorescence was performed as previously described (Shav-Tal et al., 2005). Primary antibodies used were anti-ZBP1 (IMP1) (clone 4E1, a gift of Stefan Hüttelmaier, Martin-Luther-Universität Halle, Germany), anti-Pol II (clone H14) and anti-ASF/SF2 (Zymed, San Francisco, CA). Secondary antibodies were fluorescein isothiocyanate (FITC)-labeled goat-anti-mouse IgG or IgM (Jackson ImmunoResearch, West Grove, PA, USA). Phalloidin staining was performed by incubating fixed cells with Triton X-100 for 3-4 minutes and then with TRITC-phalloidin for 1 hour.

Cells expressing CFP-actin were fixed and RNA-FISH was performed as previously described (Chartrand et al., 2000). 50-mer fluorescently labeled DNA probes were used. Cy3-MS2 against the MS2 repeats: CTAGGCAATTAGGTACCTTAGGATC-TAATGAACCCGGGAATACTGCAGAC. Cy3- or Cy5-human β-actin, a mixture of: GTGAACTTTGGGGGATGCTCGCTCCAACCGACTGCTGTCACCTTCACCGT; TCCTTAGAGAGAAGTGGGGTGGCTTTTAGGATGGCAAGGGACTTCCTGTA; CTTTTATTCAACTGGTCTCAAGTCAGTGTACAGGTAAGCCCTGGCTGCCT.

Fluorescence microscopy and data analysis

Wide-field fluorescence images were obtained using the Cell^R system containing a Z-piezo stage insert (Prior), as previously described (Aizer et al., 2008). For time-lapse imaging, cells were plated on glass-bottomed tissue culture plates (MatTek). For movie presentations, 4D image sequences were transformed into a time sequence using ImageJ by manually selecting the best plane at each time point or using the Cell^R software. For transcription site analysis, YFP-MS2 signal levels were measured using ImageJ, normalized to background and fitted with MatLab. For analysis of mRNA localization in FISH experiments, 200 cells with prominent leading edges were identified in DIC. The Cy3-labeled β-actin mRNA distribution was analyzed for each cell and the localization of their mRNA was categorized. β-actin mRNA in serum-starved cells (non-localized) surrounded the nucleus, with practically no message in the cell extremities. Localized cells were categorized as those showing: (a) a significant mRNA signal detected at the nuclear periphery and throughout the first two-thirds of the cytoplasm, together with (b) a region with reduced mRNA in last third of the cytoplasm (towards the cytoplasmic periphery); and (c) a distinct mRNA signal localizing at one side of the cell in proximity to the cytoplasmic membrane and specifically in the protruding region. The number of cells showing positive localization was counted at each time point after serum addition. For mRNP quantification in the nucleus and in the cytoplasm, the entire mRNP population in each 3D stack was detected using the Imaris particle identification tool. The images were segmented so that mRNPs were counted separately in the nucleus and cytoplasm (ImageJ). Transcription site induction was set as t=40 and the signal prior to that time point was subtracted as background.

FRAP

To study rtTA-YFP kinetics, cells were transiently transfected with rtTA-YFP using FuGENE 6 (Roche). To determine mRNP diffusion rates, cells were cotransfected with NES-YFP-MS2-NLS and CFP-LacI. Cells were imaged in phenol-red-free Leibovitz's L15 medium. The FV1000 Fluoview Olympus confocal system (1.35 NA, UPLSAPO 60×, 37°C) was used for rtTA-YFP photobleaching of free-diffusing protein. Strips of 400×52 pixels were rapidly scanned at 121 ms/frame.

For 3D FRAP of mRNP dynamics, transcription sites and long measurements of rtTA-YFP on transcription sites, images were collected using a 3D FRAP system (Photometrics) built on an Olympus IX81 microscope (63× Plan-Apo, 1.4 NA) equipped with an EM-CCD (Quant-EM, Roper), 405 and 491 nm lasers, a Lambda DG-4 light source (Sutter), *XYZ* stages (Prior) and a live-cell chamber system (Tokai), and driven by MetaMorph (Molecular Devices). For each acquisition, seven Z slices were taken at 350 nm steps. Active transcription sites were bleached using the 491 nm laser: 6 pre-bleach images, and a sequence of post-bleach images at 15 images every 2 seconds, 15 images every 6 seconds and 26 images every 30 seconds.

Experiments were analyzed using self-written ImageJ macros that sum the projected Z-stacks at every time point, and track and measure the mean intensity of the transcription site by finding the local maxima in a specific region of interest (ROI). For each time point, the background taken from a ROI outside of the cell was subtracted from all other measurements. $T_{(t)}$ and $I_{(t)}$ were measured for each time point as the average intensity of the nucleus and the average intensity in the bleached ROI, respectively. The averages of the pre-bleach images used as the initial conditions were T_i=nuclear intensity and I_i=intensity in ROI before bleaching. $Ic_{(t)}$ is the corrected intensity of the bleached ROI at time t (Phair and Misteli, 2000; Shav-Tal et al., 2004):

$$Ic_{(t)} = \frac{I_{(t)}T_i}{I_i T_{(t)}} .$$

Data from 14 cells were collected from two independent experiments and the averaged FRAP measurements were fitted to a mathematical model consisting of differential equations:

$$\frac{d[elongation]}{dt} = k_{in} + k_{-p} * [pause] - k_{out}[elongation] - k_p[elongation]$$

$$\frac{d[pause]}{dt} = k_p[elongation] - k_{-p}[pause] ,$$

using Berkeley Madonna (http://www.berkeleymadonna.com), as previously modeled (Darzacq et al., 2007). The data were fit to the model and rate constants were extracted.

For FRAP of mRNP diffusion in the cytoplasm, 5 pre-bleach images were taken, followed by 45 ms bleach with a 491 nm laser, and a sequence of post-bleach images at 60 images/500 ms and 15 images/1 second. For the bleach settings, the constants w and K were determined on fixed cells. w is the half width of the laser beam and K is a parameter describing the amount of bleaching:

$$C_{(r)} = C_i e^{-Ke^{\left(-2\frac{r^2}{w^2}\right)}},$$

where r is the radius of the bleached ROI and $C_{(r)}$ is the intensity of fluorescence along this radius after bleaching. w and K were determined simultaneously using a non-linear regression in Mathematica (Wolfram Research, Champaign, IL, USA). w and K were fitted to w=2.04236 and K=2.02371 using 11 fixed specimens. The average of 19 FRAP experiments was then fitted for γ and D using a non-linear regression in Mathematica:

$$Ic_{(t)} = \gamma\frac{1-e^{-K}}{K} + (1-\gamma)\sum_{n=0}^{40}\frac{(-K)^n}{n!}\left(1+n\left(1+\frac{2t}{w^2/4D}\right)\right)^{-1},$$

where D is the diffusion coefficient (μm^2/second) and γ is the fraction of immobile signal. The time series were averaged and the error was calculated. During mRNP bleaching, the laser and detection settings were set so that the diffuse MS2-YFP signal was below the detection level, allowing the specific detection of the mRNPs.

The transcription factor binding constant was calculated from an average of seven cells (in two independent experiments). FRAP measurements were fitted to a mathematical model consisting of differential equations using Berkeley Madonna:

$$\frac{dNuc}{dt} = P_{in} - K_{out}Nuc - K_{bind\_in}Nuc + K_{bind\_out}Site$$

$$\frac{dSite}{dt} = K_{bind\_in}Nuc - K_{bind\_out}Site\ .$$

The data for the free-diffusing population were first compared to the model to obtain the best fit, and then fit to obtain the K_{bind_in} and K_{bind_out} parameters.

Single-particle tracking

2D images over time were taken every 500 ms on the 3D FRAP system. To improve quality, we calculated and subtracted background from each frame, and activated a convolved Gaussian filter using ImageJ. mRNPs were tracked using Imaris (Bitplane). We calculated only particles appearing consistently in every frame for more than seven frames. Tracking was carried out for n=58 cytoplasmic particles from 7 different cells and n=34 nucleoplasmic particles from 5 different cells. The movement was measured per frame and the data were imported into MatLab for calculating MSD versus time and diffusion coefficients, as previously described (Saxton and Jacobson, 1997; Shav-Tal et al., 2004).

Quantitative PCR

Genomic DNA (gDNA) was isolated using the PUREGENE DNA Purification System (Gentra). For the generation of standards, a tenfold dilution was prepared. We quantified the number of integrated genes by comparison with the endogenous human β-globin gene. Primers used for the amplification of p3216PECactMS2act3UTRβ were GGATCACTCTCGGCATGGAC (forward) and TGCACATACCGGAGCCATTG (reverse). Primers used for the human β-globin reference gene were CAGTGCAGGCTGCCTATCAGA (forward) and GAATCC-AGATGCTCAAGGCCCTT (reverse). The reaction (20 μl total volume) contained 1× SYBR green mix (Thermo Scientific), 1 μl of gDNA dilution, 0.5 mM of each primer and water. The reaction was performed using the Chromo4 Real-Time Detector (Biorad) following the protocol: 15 minutes at 95°C for enzyme activation, followed by 40 cycles consisting of 15 seconds denaturation at 92°C, 10 seconds annealing at 64°C and 20 seconds extension at 72°C. The fluorescent signal was measured at the end of each cycle. A final dissociation stage was performed to generate a melting curve for verification of amplification product specificity. For calculating the gene copy number, we calculated the reaction efficiency for each set of primers using five dilutions of gDNA (triplicates) and Opticon2 software (Bio-Rad). We measured the average cycle number for each gDNA sample using both primer sets and calculated the concentration (Q_c) of each reaction by: $Q_c = efficiency^{-cycle\_time}$. Then, we could calculate the gene copy number of the samples:

$$\frac{Q_c(CFP\_primers)}{Q_c(beta\_globin)/2}.$$

We verified that the U2OS cell line has only two alleles of the β-globin gene by comparison with a non-cancerous cell line.

We thank Stefan Hüttelmaier for the anti-ZBP1 (IMP1) antibody and Alex Perlman for help with qPCR. This work was supported by the United States-Israel Binational Science Foundation (Y.S.-T. and R.H.S.), the Israel Science Foundation (Y.S.-T.) the Israel Health Ministry (Y.S.-T.), the Alon Fellowship (Y.S.-T.), NIH grant EB2060 (R.H.S.) and NIGMS grant 42694 (D.L.S.). Y.S.-T. thanks the Israel Science Foundation for the fluorescence live-cell imaging microscope. Y.S.-T. is the Jane Stern Lebell Family Fellow in Life Sciences at Bar-Ilan University. Y.B. is grateful to the Azrieli Foundation for the award of an Azrieli Fellowship. Deposited in PMC for release after 12 months.

Supplementary material available online at
http://jcs.biologists.org/cgi/content/full/123/10/1761/DC1

References

Aizer, A., Brody, Y., Ler, L. W., Sonenberg, N., Singer, R. H. and Shav-Tal, Y. (2008). The dynamics of mammalian P body transport, assembly, and disassembly in vivo. *Mol. Biol. Cell* **19**, 4154-4166.

Archer, T. K., Lee, H. L., Cordingley, M. G., Mymryk, J. S., Fragoso, G., Berard, D. S. and Hager, G. L. (1994). Differential steroid hormone induction of transcription from the mouse mammary tumor virus promoter. *Mol. Endocrinol.* **8**, 568-576.

Bassell, G. J., Singer, R. H. and Kosik, K. S. (1994). Association of poly(A) mRNA with microtubules in cultured neurons. *Neuron* **12**, 571-582.

Bassell, G. J., Oleynikov, Y. and Singer, R. H. (1999). The travels of mRNAs through all cells large and small. *FASEB J.* **13**, 447-454.

Bentley, D. L. (2005). Rules of engagement: co-transcriptional recruitment of pre-mRNA processing factors. *Curr. Opin. Cell Biol.* **17**, 251-256.

Boireau, S., Maiuri, P., Basyuk, E., de la Mata, M., Knezevich, A., Pradet-Balade, B., Backer, V., Kornblihtt, A., Marcello, A. and Bertrand, E. (2007). The transcriptional cycle of HIV-1 in real-time and live cells. *J. Cell Biol.* **179**, 291-304.

Braga, J., Rino, J. and Carmo-Fonseca, M. (2004). Photobleaching microscopy reveals the dynamics of mRNA-binding proteins inside live cell nuclei. *Prog. Mol. Subcell. Biol.* **35**, 119-134.

Braga, J., McNally, J. G. and Carmo-Fonseca, M. (2007). A reaction-diffusion model to study RNA motion by quantitative fluorescence recovery after photobleaching. *Biophys. J.* **92**, 2694-2703.

Calapez, A., Pereira, H. M., Calado, A., Braga, J., Rino, J., Carvalho, C., Tavanez, J. P., Wahle, E., Rosa, A. C. and Carmo-Fonseca, M. (2002). The intranuclear mobility of messenger RNA binding proteins is ATP dependent and temperature sensitive. *J. Cell Biol.* **159**, 795-805.

Chartrand, P., Bertrand, E., Singer, R. H. and Long, R. M. (2000). Sensitive and high-resolution detection of RNA in situ. *Methods Enzymol.* **318**, 493-506.

Chubb, J. R., Trcek, T., Shenoy, S. M. and Singer, R. H. (2006). Transcriptional pulsing of a developmental gene. *Curr. Biol.* **16**, 1018-1025.

Condeelis, J. and Singer, R. H. (2005). How and why does beta-actin mRNA target? *Biol. Cell* **97**, 97-110.

Darzacq, X., Shav-Tal, Y., de Turris, V., Brody, Y., Shenoy, S. M., Phair, R. D. and Singer, R. H. (2007). In vivo dynamics of RNA polymerase II transcription. *Nat. Struct. Mol. Biol.* **14**, 796-806.

Dundr, M., Hoffmann-Rohrer, U., Hu, Q., Grummt, I., Rothblum, L. I., Phair, R. D. and Misteli, T. (2002). A kinetic framework for a mammalian RNA polymerase in vivo. *Science* **298**, 1623-1626.

Femino, A. M., Fay, F. S., Fogarty, K. and Singer, R. H. (1998). Visualization of single RNA transcripts in situ. *Science* **280**, 585-590.

Fusco, D., Accornero, N., Lavoie, B., Shenoy, S. M., Blanchard, J. M., Singer, R. H. and Bertrand, E. (2003). Single mRNA molecules demonstrate probabilistic movement in living mammalian cells. *Curr. Biol.* **13**, 161-167.

Golding, I. and Cox, E. C. (2004). RNA dynamics in live Escherichia coli cells. *Proc. Natl. Acad. Sci. USA* **101**, 11310-11315.

Golding, I., Paulsson, J., Zawilski, S. M. and Cox, E. C. (2005). Real-time kinetics of gene activity in individual bacteria. *Cell* **123**, 1025-1036.

Hager, G. L., McNally, J. G. and Misteli, T. (2009). Transcription dynamics. *Mol. Cell* **35**, 741-753.

Hirose, Y. and Manley, J. L. (2000). RNA polymerase II and the integration of nuclear events. *Genes Dev.* **14**, 1415-1429.

Hofer, D., Ness, W. and Drenckhahn, D. (1997). Sorting of actin isoforms in chicken auditory hair cells. *J. Cell Sci.* **110**, 765-770.

Hotulainen, P. and Lappalainen, P. (2006). Stress fibers are generated by two distinct actin assembly mechanisms in motile cells. *J. Cell Biol.* **173**, 383-394.

Huttelmaier, S., Zenklusen, D., Lederer, M., Dictenberg, J., Lorenz, M., Meng, X., Bassell, G. J., Condeelis, J. and Singer, R. H. (2005). Spatial regulation of beta-actin translation by Src-dependent phosphorylation of ZBP1. *Nature* **438**, 512-515.

Iborra, F. J., Pombo, A., Jackson, D. A. and Cook, P. R. (1996). Active RNA polymerases are localized within discrete transcription 'factories' in human nuclei. *J. Cell Sci.* **109**, 1427-1436.

Janicki, S. M. and Spector, D. L. (2003). Nuclear choreography: interpretations from living cells. *Curr. Opin. Cell Biol.* **15**, 149-157.

Janicki, S. M., Tsukamoto, T., Salghetti, S. E., Tansey, W. P., Sachidanandam, R., Prasanth, K. V., Ried, T., Shav-Tal, Y., Bertrand, E., Singer, R. H. et al. (2004). From silencing to gene expression; real-time analysis in single cells. *Cell* **116**, 683-698.

Juven-Gershon, T., Hsu, J. Y., Theisen, J. W. and Kadonaga, J. T. (2008). The RNA polymerase II core promoter-the gateway to transcription. *Curr. Opin. Cell Biol.* **20**, 253-259.

Khyrul, W. A., LaLonde, D. P., Brown, M. C., Levinson, H. and Turner, C. E. (2004). The integrin-linked kinase regulates cell morphology and motility in a rho-associated kinase-dependent manner. *J. Biol. Chem.* **279**, 54131-54139.

Kiebler, M. A. and Bassell, G. J. (2006). Neuronal RNA granules: movers and makers. *Neuron* **51**, 685-690.
Kislauskis, E. H., Li, Z., Singer, R. H. and Taneja, K. L. (1993). Isoform-specific 3′-untranslated sequences sort alpha-cardiac and beta-cytoplasmic actin messenger RNAs to different cytoplasmic compartments. *J. Cell Biol.* **123**, 165-172.
Kislauskis, E. H., Zhu, X. and Singer, R. H. (1994). Sequences responsible for intracellular localization of beta-actin messenger RNA also affect cell phenotype. *J. Cell Biol.* **127**, 441-451.
Kohler, A. and Hurt, E. (2007). Exporting RNA from the nucleus to the cytoplasm. *Nat. Rev. Mol. Cell Biol.* **8**, 761-773.
Latham, V. M., Jr, Kislauskis, E. H., Singer, R. H. and Ross, A. F. (1994). Beta-actin mRNA localization is regulated by signal transduction mechanisms. *J. Cell Biol.* **126**, 1211-1219.
Lawrence, J. B. and Singer, R. H. (1986). Intracellular localization of messenger RNAs for cytoskeletal proteins. *Cell* **45**, 407-415.
Maniatis, T. and Reed, R. (2002). An extensive network of coupling among gene expression machines. *Nature* **416**, 499-506.
Moore, M. J. (2005). From birth to death: the complex lives of eukaryotic mRNAs. *Science* **309**, 1514-1518.
Moore, M. J. and Proudfoot, N. J. (2009). Pre-mRNA processing reaches back to transcription and ahead to translation. *Cell* **136**, 688-700.
Muller, W. G., Walker, D., Hager, G. L. and McNally, J. G. (2001). Large-scale chromatin decondensation and recondensation regulated by transcription from a natural promoter. *J. Cell Biol.* **154**, 33-48.
Neugebauer, K. M. (2002). On the importance of being co-transcriptional. *J. Cell Sci.* **115**, 3865-3871.
Phair, R. D. and Misteli, T. (2000). High mobility of proteins in the mammalian cell nucleus. *Nature* **404**, 604-609.
Politz, J. C. and Pederson, T. (2000). Review: movement of mRNA from transcription site to nuclear pores. *J. Struct. Biol.* **129**, 252-257.
Pombo, A., Jones, E., Iborra, F. J., Kimura, H., Sugaya, K., Cook, P. R. and Jackson, D. A. (2000). Specialized transcription factories within mammalian nuclei. *Crit. Rev. Eukaryot. Gene Expr.* **10**, 21-29.
Ross, A. F., Oleynikov, Y., Kislauskis, E. H., Taneja, K. L. and Singer, R. H. (1997). Characterization of a beta-actin mRNA zipcode-binding protein. *Mol. Cell. Biol.* **17**, 2158-2165.
Saxton, M. J. and Jacobson, K. (1997). Single-particle tracking: applications to membrane dynamics. *Annu. Rev. Biophys. Biomol. Struct.* **26**, 373-399.
Shav-Tal, Y. and Singer, R. H. (2005). RNA localization. *J. Cell Sci.* **118**, 4077-4081.
Shav-Tal, Y. and Gruenbaum, Y. (2009). Single-molecule dynamics of nuclear mRNA. *F1000 Biology Reports* **1**, 29-32.
Shav-Tal, Y., Darzacq, X., Shenoy, S. M., Fusco, D., Janicki, S. M., Spector, D. L. and Singer, R. H. (2004). Dynamics of single mRNPs in nuclei of living cells. *Science* **304**, 1797-1800.
Shav-Tal, Y., Blechman, J., Darzacq, X., Montagna, C., Dye, B. T., Patton, J. G., Singer, R. H. and Zipori, D. (2005). Dynamic sorting of nuclear components into distinct nucleolar caps during transcriptional inhibition. *Mol. Biol. Cell* **16**, 2395-2413.
Shav-Tal, Y., Darzacq, X. and Singer, R. H. (2006). Gene expression within a dynamic nuclear landscape. *EMBO J.* **25**, 3469-3479.
Shestakova, E. A., Singer, R. H. and Condeelis, J. (2001). The physiological significance of beta-actin mRNA localization in determining cell polarity and directional motility. *Proc. Natl. Acad. Sci. USA* **98**, 7045-7050.
Singh, J. and Padgett, R. A. (2009). Rates of in situ transcription and splicing in large human genes. *Nat. Struct. Mol. Biol.* **16**, 1128-1133.
Sprague, B. L., Pego, R. L., Stavreva, D. A. and McNally, J. G. (2004). Analysis of binding reactions by fluorescence recovery after photobleaching. *Biophys. J.* **86**, 3473-3495.
Sundell, C. L. and Singer, R. H. (1991). Requirement of microfilaments in sorting of actin messenger RNA. *Science* **253**, 1275-1277.
Sutherland, H. and Bickmore, W. A. (2009). Transcription factories: gene expression in unions? *Nat. Rev. Genet.* **10**, 457-466.
Tsukamoto, T., Hashiguchi, N., Janicki, S. M., Tumbar, T., Belmont, A. S. and Spector, D. L. (2000). Visualization of gene activity in living cells. *Nat. Cell Biol.* **2**, 871-878.
Tumbar, T., Sudlow, G. and Belmont, A. S. (1999). Large-scale chromatin unfolding and remodeling induced by VP16 acidic activation domain. *J. Cell Biol.* **145**, 1341-1354.
Tyagi, S. and Alsmadi, O. (2004). Imaging native beta-actin mRNA in motile fibroblasts. *Biophys. J.* **87**, 4153-4162.
Vargas, D. Y., Raj, A., Marras, S. A., Kramer, F. R. and Tyagi, S. (2005). Mechanism of mRNA transport in the nucleus. *Proc. Natl. Acad. Sci. USA* **102**, 17008-17013.
Vikesaa, J., Hansen, T. V., Jonson, L., Borup, R., Wewer, U. M., Christiansen, J. and Nielsen, F. C. (2006). RNA-binding IMPs promote cell adhesion and invadopodia formation. *EMBO J.* **25**, 1456-1468.
Wada, Y., Ohta, Y., Xu, M., Tsutsumi, S., Minami, T., Inoue, K., Komura, D., Kitakami, J., Oshida, N., Papantonis, A. et al. (2009). A wave of nascent transcription on activated human genes. *Proc. Natl. Acad. Sci. USA* **106**, 18357-18361.
Yisraeli, J. K. (2005). VICKZ proteins: a multi-talented family of regulatory RNA-binding proteins. *Biol. Cell* **97**, 87-96.